OATAO
Open Archive Toulouse Archive Ouverte

Open Archive Toulouse Archive Ouverte (OATAO)

OATAO is an open access repository that collects the work of some Toulouse researchers and makes it freely available over the web where possible.

This is an author's   version published in: https://oatao.univ-toulouse.fr/28445

To cite this version :

Any correspondence concerning this service should be sent to the repository administrator:
tech-oatao@listes-diff.inp-toulouse.fr

AN ANALYTICAL MODEL FOR PROPELLER AERODYNAMIC EFFORTS AT HIGH INCIDENCE

Yuchen Leng[(1), (2)], Jean-Marc Moschetta[(1)], Thierry Jardin[(1)] and Murat Bronz[(3)]
[(1)]*ISAE-SUPAERO, Université de Toulouse, France, yuchen.leng@isae-supaero.fr*
[(2)]*Delair, 676 Rue Max Planck, 31670 Labège, France, yuchen.leng@delair.aero*
[(3)]*ENAC, Université de Toulouse, France, murat.bronz@enac.fr*

ABSTRACT

In the advent of electrical vertical take-off and landing aircraft development, a fast approach to predict variation of propeller axial and off-axis aerodynamic loads at large incidence angle has been desired. This paper presented an analytical approach obtained by a simplified blade element method considering local blade section conditions. The theory has been further validated against available experiments for propeller at high incidence conditions, and was found applicable to a wide range of geometries and operating conditions.

1. INTRODUCTION

With the advance in electric propulsion technologies, Vertical Take-Off and Landing (VTOL) aerial vehicles have gained renewed interest thanks to its flexibility in constrained mission environment. Several concepts of VTOL aircraft have been proposed. Convertible un-manned aerial vehicles (UAV), such as MAVION developed at ISAE or Cyclone from ENAC shown in Fig. 1, have demonstrated operational advantages in its convenience of recovery. To fully exploit the potential of VTOL operations, a good understanding of the flight dynamics during transition between hover and cruise is critical. Apart from complex aerodynamic phenomena presented over lifting surfaces, propeller also experiences large incidence angle due to unusual attitude. Operating away from its design conditions, the propeller produces extra off-axis forces and moments that affect transition flight characteristics greatly.

(a) ISAE MAVION [9]   (b) ENAC Cyclone [1]

Figure 1: VTOL UAV concepts

1.1 Background

The additional aerodynamic efforts induced by propeller incidence angle have raised the attention of early aeronautical researchers. Harris [5] and Glauert [4] have obtained analytical solutions of ratios between propeller efforts at incidence and their values in axisymmetric conditions. Their methods modelled the variation in thrust and torque coefficient, and then formulated the off-axis efforts in relation to thrust and torque. However, their models are generic and don't take the specific geometry of the propeller into account.

In 1945, Herbert S Ribner has published his analytical model for propeller at incidence. The results have been published in two technical reports of National Advisory Committee for Aeronautics (NACA) [12, 13]. Ribner's model considered the blade planform shape. He took the blade projected area perpendicular to propeller disk as a fin in side-slip, and derived side force contribution from a vertical fin analogy. The results were in good agreement for moderate incidence angle up to $20°$.

De Young further extended Ribner's model for high incidence cases in an 1965 research [2]. Approximations were applied to integrations in Ribner's derivation to simplify calculation without compromise in accuracy, and the tangential of incidence angle were multiplied for normal force and yaw moment at high incidence. The results however diverges at $90°$, or edge-wise flow.

The development of numerical method enabled more detailed analysis based on either blade element theory (BET) or numerical solution of Navier-Stokes equations. Notable researches include the blade element momentum theory formulated by Leishman [6], dynamic inflow model for helicopter rotor by Pitt and Peters [10]. A more recent blade element study by Leng et al [8] observed several particular aerodynamic phenomena associated with high incidence flight condition. Stall delay model and inflow model were determined to be critical in achieving good correlation with experimental data. Despite the advancements, these numerical methods were costly to be integrated into a full-vehicle optimisation routine.

1.2 Current work

In view of the past studies, an analytical model is desired for full-vehicle optimisation, which focuses on preliminary sizing of a convertible aircraft. The new model mod-

ified the previous theory from De Young to be suitable for low-speed and hover conditions, where normalisation with freestream velocity may not be appropriate. A new correction for off-axis efforts at high incidence angles has also been derived to attain closer agreement with existing experimental data [7, 15].
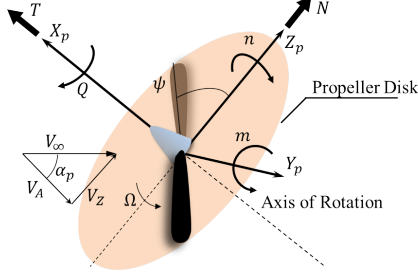

Figure 2: Aerodynamic loads on a propeller at incidence

The current study has modelled the variations of four propeller efforts shown in Fig. 2: axial efforts including thrust T, torque Q (measured as power $P = Q\Omega$), and off-axis efforts containing normal force N and yaw moment n as a function of incidence angle α_p. α_p is defined to be the angle between wind direction and propeller axis of rotation.

The forces and moments acting on the propeller are decomposed following aircraft convention for rotor installed along longitudinal axis: T and Q are aligned with rotation axis X_p; N and n are in-line with the downstream direction of freestream component on propeller disk V_Z.

2. PROPELLER BLADE ELEMENT ANALYSIS

To better elucidate the formulation of analytical model, it is imperative to understand the main contribution of aerodynamic loads present on the propeller blade. This section will briefly introduce a blade element analysis on the origins of blade sectional load. Axial flight condition will first be analysed and then expanded to conditions with non-zero incidence.

2.1 Axial flight condition

A single propeller will be considered immersed in uniform freestream whose direction is parallel to rotation axis. Under such assumption, each blade section at the same radius from hub should encounter identical flow condition, and thus the flowfield is axisymmetric. The analysis will be limited to low speed condition, hence incompressible flow.

Consider a blade section along the circumference at radius r from axis of rotation. Its orientation could be defined in relation to rotor disk plane. The local pitch angle

β will be defined as the angle between sectional zero-lift line and the rotor disk plane, in the same fashion as Phillips [11].
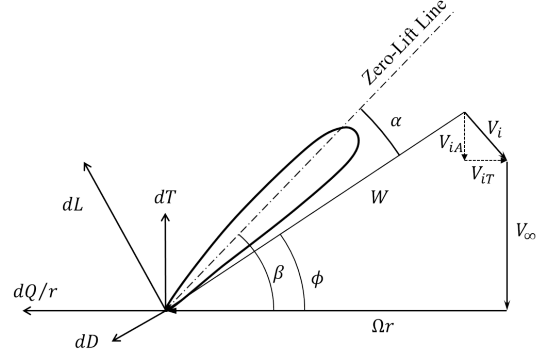

Figure 3: Blade section in axial flow

As the blade rotates, two major components of flow velocity can be seen in Fig. 3. Firstly, the freestream component V_∞ and secondly the velocity in rotor disk plane due to rotation Ωr.

Besides V_∞ and Ωr, velocity V_i induced by the production of thrust and torque on the propeller blade is also depicted in Fig. 3. To produce forward thrust, momentum must be added to the fluid in axial direction, and thus creating an incremental velocity component in the rotation axis V_{i_A}. To keep propeller turning, a torque must be supplied, and similarly a tangential flow component V_{i_T} is induced due to the exchange of angular momentum.

The local effective wind velocity W is the vector sum of all the components encountered by the depicted blade element. The angle between W and propeller disk plane is inflow angle ϕ. The difference between blade pitch and inflow angle gives local angle of attack $\alpha = \beta - \phi$.

The lift and drag of the blade section can be resolved in directions perpendicular and parallel to the effective wind respectively, taking into account of chord Reynolds number and local angle of attack. They can then be transferred into sectional thrust and torque.

$$
\begin{aligned}
dT &= \frac{1}{2}\rho W^2 c \left(C_L \cos\phi - C_D \sin\phi\right) dr \\
dQ &= \frac{1}{2}\rho W^2 c \left(C_L \cos\phi - C_D \sin\phi\right) r dr
\end{aligned}
\tag{1}
$$

Propeller thrust and torque can be found by integrating Eq. 1 along each blade radius.

Because of the axisymmetric flow condition, the analysis doesn't depend on the azimuthal position of blade.

2.2 Non-zero incidence angle

When the angle α_p becomes non-zero, the propeller is at incidence. The freestream can be decomposed as an axial component $V_A = V_\infty \cos \alpha_p$ and an in-plane component $V_Z = V_\infty \sin \alpha_p$. V_A gives a reduced freestream effect in axial direction and V_Z causes a variation of flow condition in azimuthal direction.
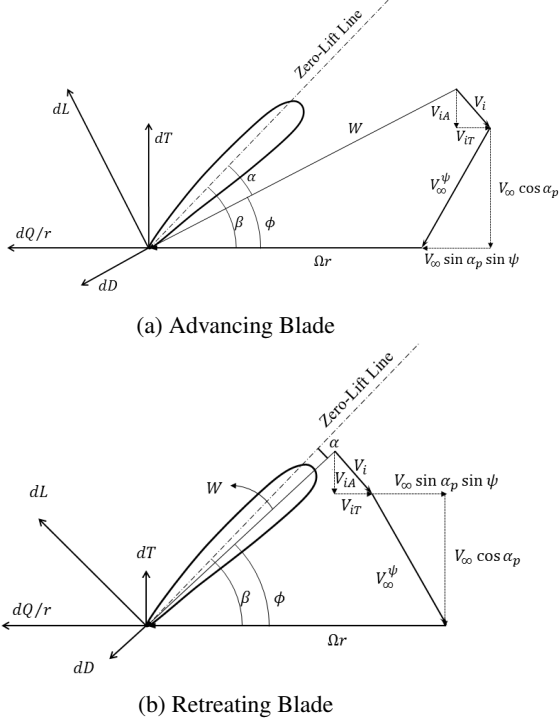

(a) Advancing Blade

(b) Retreating Blade

Figure 4: Flow directions of advancing and retreating blade sections

Blade element analysis for non-zero incidence angle follows the same fashion except that most flow components vary with blade azimuthal position ψ, which is defined to be zero when the blade span-wise direction coincides with V_Z.

Flow conditions for a blade section on two sides of propeller are illustrated in Fig. 4.

On advancing side of the propeller, where $0 < \psi < \pi$, the projection of in-plane component is in the same direction of blade rotation. Its effect is to increase local relative wind speed and angle of attack. The opposite is true for the other retreating side, where $\pi < \psi < 2\pi$. Both local thrust and tangential force change with azimuthal angle as a consequence of this local flow condition variation.

3. THRUST AND POWER COEFFICIENTS

The thrust and power coefficients, defined as

$$C_T = \frac{4\pi^2 T}{\rho \Omega^2 D^4} \tag{2}$$

$$C_P = \frac{8\pi^3 Q}{\rho \Omega^2 D^5} \tag{3}$$

where Ω is magnitude of angular velocity in radians per second and D is propeller diameter, have been well studied for axisymmetric conditions, a semi-empirical estimation for an arbitrary propeller can be found in [14]. For fixed-pitch configuration at zero incidence angle, the coefficients mainly depend on advance ratio $J = 2\pi \frac{V_\infty}{\Omega D}$, which is proportional to the ratio of freestream velocity and the propeller tip speed. Von Mises [14] have suggested a linear approximation for thrust and power coefficients :

$$C_T = K \pi \bar{r}' \sigma \cos \beta' (J_{0T} - J) \tag{4}$$

$$C_P = K \left(\pi \bar{r}' \right)^2 \sigma \sin \beta' (J_{0P} - J) \tag{5}$$

where K is an empirical constant and $\bar{r}'$ is the position of representative section in percentage radius (generally 75%). The solidity σ and pitch angle β' are evaluated at the representative section. Two important parameters are J_{0T} and J_{0P}, they are the advance ratios where the thrust and power coefficients reach zero respectively. They can be interpolated graphically or estimated empirically [14].

Based on this approximation and local blade analysis, De Young has proposed an analytical approach to express thrust and power coefficients at non-zero incidence angle as ratios to their respective values in a representative axisymmetric condition with advance ratio $J \cos \alpha_p$.

$$\eta_T = \frac{C_T(\alpha_p, J)}{C_T(0, J \cos \alpha_p)} \tag{6}$$

$$\eta_P = \frac{C_P(\alpha_p, J)}{C_P(0, J \cos \alpha_p)} \tag{7}$$

This method proves to be sufficiently accurate even for high incidence angle and it forms the basis for off-axis efforts modelling, and thus will be briefly presented in this section.

3.1 Local advance ratio

As seen in section 2, the inflow angle ϕ varies with blade azimuthal position at non-zero incidence angle. It reaches minimum at $\psi = 90°$ and maximum at $\psi = 270°$. This variation of inflow angle ϕ results in a change of local advance ratio at representative blade section.

$$J_{local} = \frac{J \cos \alpha_p}{1 + J \sin \alpha_p \sin \psi / \pi \bar{r}'} \tag{8}$$

3

We also denote three particular local advance ratios at $\psi = 0°, 90°$ and $270°$.

$$J_{base} = J\cos\alpha_p \qquad (9)$$

$$J_{min} = \frac{J\cos\alpha_p}{1 + J\sin\alpha_p/\pi\bar{r}'} \qquad (10)$$

$$J_{max} = \frac{J\cos\alpha_p}{1 - J\sin\alpha_p/\pi\bar{r}'} \qquad (11)$$

From Von Mises' linear approximations, the local thrust coefficient can be related to freestream dynamic pressure and local advance ratio.

$$C_T(\psi) = K\pi\bar{r}'\sigma\cos\beta'\left(J_{0T} - J_{local}\right)\left(\frac{J_{axial}}{J_{local}}\right)^2 \qquad (12)$$

where $J_{axial} = J\cos\alpha_p$.

3.2 Thrust and power ratios

Variations in blade angle of attack and dynamic pressure induces azimuthal load variation, which could be approximated by a 2-harmonic cosine series [2].

$$\tilde{C}_T(\psi) = A_0 + A_1\cos\left(\psi - \frac{\pi}{2}\right) \\ + A_2\cos 2\left(\psi - \frac{\pi}{2}\right) \qquad (13)$$

The curve notably has several characteristic points :

$$\begin{aligned} C_{T_{base}} &= A_0 - A_2 & \psi &= 0 \\ C_{T_{max}} &= A_0 + A_1 + A_2 & \psi &= \frac{\pi}{2} \\ C_{T_{min}} &= A_0 - A_1 + A_2 & \psi &= \frac{3\pi}{2} \end{aligned} \qquad (14)$$

This approximation, though not exact, is a reasonable description of sectional thrust variation, as seen in Fig. 5. The curve depict thrust variation at different azimuthal positions of one blade section situated at 76%R for a constant chord propeller having NACA0012 airfoil, and is in the high pitch configuration tested in [7]. The analysis was performed at a typical condition with moderate advance ratio $J = 0.45$ and medium incidence $\alpha_p = 45°$.

The solid line was obtained by performing blade element analysis with a dynamic inflow model. The dash line is the 2-harmonic cosine series approximation by using the characteristic points calculated from blade element theory. The estimation is reasonable for downstream blade, while the upstream blade thrust is underestimated. The difference is caused by variation of induced velocity in longitudinal direction, which tends to increase local angle of attack for upstream blade.

The averaged thrust within one revolution can be represented by thrust condition at the characteristic points.
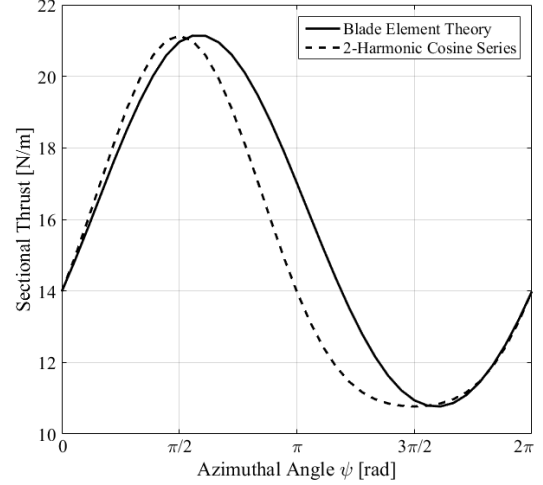

Figure 5: Comparison between a blade element solution of thrust variation and cosine approximation

$$\begin{aligned} C_T &= \frac{1}{2\pi}\int_0^{2\pi} \tilde{C}_T(\psi)\,d\psi \\ &= \frac{1}{2\pi}\int_0^{2\pi} A_0 + A_1\cos\left(\psi - \frac{\pi}{2}\right) \\ &\qquad + A_2\cos\left(2\psi - \pi\right)d\psi \\ &= A_0 = \frac{1}{4}\left(2C_{T_{base}} + C_{T_{min}} + C_{T_{max}}\right) \end{aligned} \qquad (15)$$

Assume the maximal, mean and minimal thrust coefficients correspond to the minimal, mean and maximal advance ratios respectively.

$$\begin{aligned} C_{T_{max}} &= K\pi\bar{r}'\sigma\cos\beta'\left(J_{0T} - J_{min}\right)\left(\frac{J\cos\alpha_p}{J_{min}}\right)^2 \\ C_{T_{base}} &= K\pi\bar{r}'\sigma\cos\beta'\left(J_{0T} - J_{base}\right)\left(\frac{J\cos\alpha_p}{J_{base}}\right)^2 \\ C_{T_{min}} &= K\pi\bar{r}'\sigma\cos\beta'\left(J_{0T} - J_{max}\right)\left(\frac{J\cos\alpha_p}{J_{max}}\right)^2 \end{aligned} \qquad (16)$$

Substitute the local advance ratios from Eqs. 9-11, and insert Eq. 16 into Eq. 15, the averaged thrust coefficient at total advance ratio J and incidence angle α_p can be obtained.

$$C_T(\alpha_p, J) = K\pi\bar{r}'\sigma\cos\beta' \\ \left[J_{0T} - J\cos\alpha_p + \frac{J_{0T}}{2}\left(\frac{J\sin\alpha_p}{\pi\bar{r}'}\right)^2\right] \qquad (17)$$

Notice that the first term in Eq. 17 is identical to the thrust at zero incidence with a reduced advance ratio at

4

exactly $J \cos \alpha_p$. Divided by the thrust coefficient at the corresponding axisymmetric condition, an expression for the thrust ratio can be resolved.

$$\eta_T = 1 + \frac{(J \sin \alpha_p / \pi \bar{r}')^2}{2 (1 - J \cos \alpha_p / J_{0T})} \qquad (18)$$

Similarly power ratio can also be obtained.

$$\eta_P = 1 + \frac{(J \sin \alpha_p / \pi \bar{r}')^2}{2 (1 - J \cos \alpha_p / J_{0P})} \qquad (19)$$

A final correction to thrust and power ratios were added in [2] to make them consistent with analysis of helicopter rotor in forward flight condition [3]. The second term in thrust and power ratios is multiplied by a solidity term, which increases with incidence and diminishes to unity at $\alpha_p = 0$.

$$\delta(\alpha_p) = \frac{3}{2} \cos \beta'$$
$$\left[1 + \frac{\sigma'}{\tan \beta'} \left(1 + \sqrt{1 + \frac{2 \tan \beta'}{\sigma'}} \right) (1 - \cos \alpha_p) \right] \qquad (20)$$

The corrected thrust and power ratios are given in Eqs. 21, 22

$$\eta_T = 1 + \frac{(J \sin \alpha_p / \pi \bar{r}')^2}{2 (1 - J \cos \alpha_p / J_{0T})} \delta(\alpha_p) \qquad (21)$$

$$\eta_P = 1 + \frac{(J \sin \alpha_p / \pi \bar{r}')^2}{2 (1 - J \cos \alpha_p / J_{0P})} \delta(\alpha_p) \qquad (22)$$

3.3 Validation of analytical expressions for thrust and power

The theory has been compared with two different sets of experimental data. The first database was published in 1960 from Yaggy et al [15]. Thrust and power coefficients as well as off-axis efforts were measured from three full-scale aircraft propellers at high incidence angle up to 85°. Geometry data was also published allowing for model validation, although the lack of detailed test condition (rotation speed or freestream velocity) prevents such validation to be comprehensive. The data for the Curtiss C634S-C500 propeller (referred to as No.1 propeller) at pitch setting $\beta' = 35°$ is compared against the theory. Interested readers are kindly referred to NACA technical report D-318 [15] for detailed information.

Data was extrapolated for four advance ratios $J = 0.3, 0.5, 0.7$ and 0.9. Thrust data was plotted in Fig. 6 against incidence angle, where experimental data was shown in different markers and theoretical predictions in lines. As expected from classic propeller analysis, at axial conditions, the thrust coefficient decreases with advance ratio. The theoretical value matches exactly with

experimental results since the thrust ratio η_T is unity at zero incidence. With increasing α_p thrust starts to rise gently initially, and more drastically at higher incidence. The variation is larger at high advance ratio.
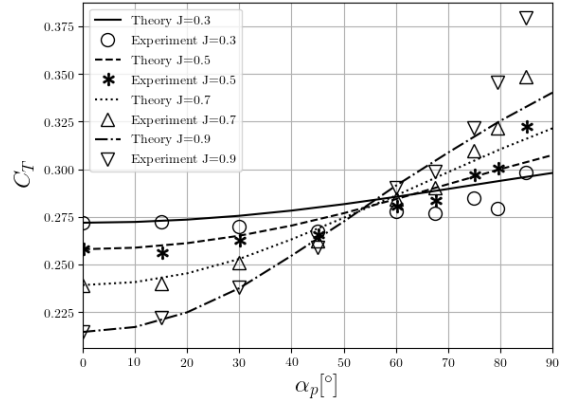

Figure 6: Thrust coefficient of No.1 propeller in [15] against incidence angle for various advance ratios

For all advance ratios, the estimations from analytical model follows the experimental results closely, until a convergence region around $\alpha_p = 60°$, where all curves seem to pass through. Above this angle, the theory underestimates thrust coefficient at high advance ratio.
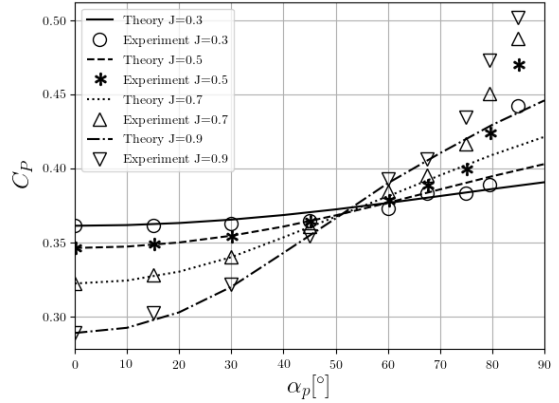

Figure 7: Power coefficient of No.1 propeller in [15] against incidence angle for various advance ratios

In Fig. 7 power coefficients were plotted in a similar fashion. The trend is consistent with that observed in Fig. 6. A slightly lower convergence region exists for power coefficient curves, and above it, the theoretical value at high advance ratio is lower compared to experimental results.

From the validation, it can be concluded for the case of No.1 propeller in Yaggy's experiment, the analytical model applies well for various combinations of advance ratio and incidence angle. It also explains well the increasing amplitude of thrust and power coefficients at higher advance ratio. For a given incidence angle, the

thrust and power ratios in Eqs. 21, 22 can be written in the form of Eqs. 23, 24.

$$\eta_T = 1 + \frac{J\left(\sin\alpha_p/\pi\bar{r}'\right)^2}{2\left(1/J - \cos\alpha_p/J_{0T}\right)}\delta\left(\alpha_p\right) \qquad (23)$$

$$\eta_P = 1 + \frac{J\left(\sin\alpha_p/\pi\bar{r}'\right)^2}{2\left(1/J - \cos\alpha_p/J_{0P}\right)}\delta\left(\alpha_p\right) \qquad (24)$$

As advance ratio increases, the numerator is proportional with J, while the first term in denominator reduces. Thus the thrust and power ratios increase faster with advance ratio than a linear function.

The second experimental database is a recent small-scale propeller test performed at ISAE-SUPAERO low-Reynolds number wind tunnel (SaBRe). The test was dedicated to convertible drone research [7]. Both test condition and results are available for comparison. Model validation of the current study has been performed over the experimental data of high pitch propeller.
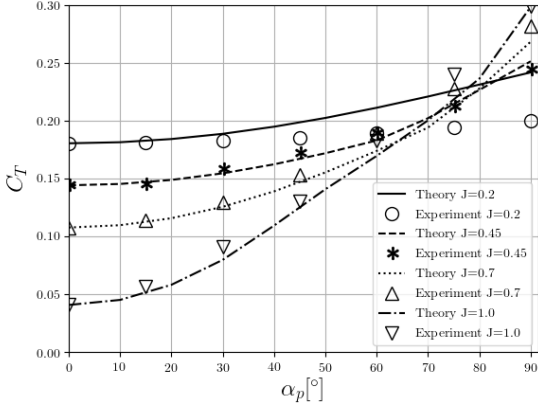

Figure 8: Thrust coefficient of a small-scale propeller against incidence angle for various advance ratios

In Fig. 8, the thrust coefficient was compared between the analytical model and the experimental data, for advance ratio 0.2, 0.45, 0.7 and 1.0. Theoretical results plotted in lines were extrapolated from coefficients obtained in experiments at zero incidence angle.

The theoretical results agreed reasonably well for all tested conditions, particularly at smaller advance ratios. The initial increase in thrust coefficient is gentle, while the curves start to steepen as incidence increases. The gradient is more significant at higher advance ratio and the theoretical model tends to underestimate, resulting conservative thrust value.

The comparison for power coefficient is depicted in Fig. 9. The non-linear trend is very similar to that of thrust coefficient. The irregularities exhibited in the plot are traced to the lack of axial experimental data to interpolate power coefficients at representative axisymmetric conditions.
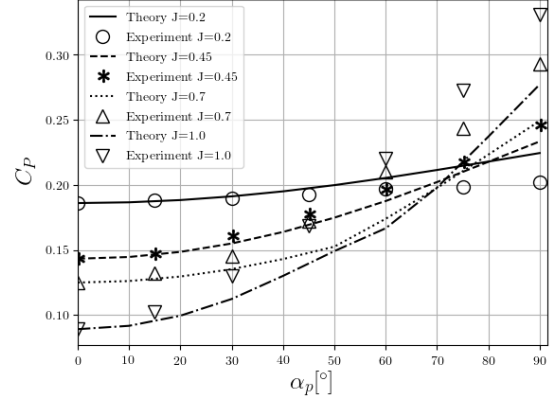

Figure 9: Power coefficient of a small-scale propeller against incidence angle for various advance ratios

The analytical model similarly underestimated the gradient of power coefficient against incidence angle. This error in both thrust and power coefficient might be attributed to the influence of higher order terms, which are neglected while obtaining the linear thrust and power characteristics.

4. OFF-AXIS EFFORTS

Besides the increase in thrust and power with incidence angle, extra off-axis efforts appear as a result of non-uniform blade loading. The most significant components are the normal force and yaw moment [11, 13], and are expressed as non-dimensional coefficients in Eqs. 25, 26.

$$C_N = \frac{4\pi^2 N}{\rho\Omega^2 D^4} \qquad (25)$$

$$C_n = \frac{4\pi^2 n}{\rho\Omega^2 D^5} \qquad (26)$$

An analytical approach has been obtained as a linear approximation for small incidence angle by Ribner [12, 13]. De Young later extended the estimation to high incidence cases [2]. The normal force and yaw moment were modelled as ratios to their respective gradient at zero incidence angle, which were obtained using Ribner's theory. De Young derived these ratios to be $\tan\alpha_p$, which is actually incorrect. The error results in singularity at 90° incidence angle and significant overestimation at high incidence angle.

Ribner's theory for off-axis effort gradients at small incidence will be presented in this section firstly in a form suitable for low-speed / hover condition. A correct evaluation of normal force and yaw moment in relation to their gradients at zero incidence will then be presented. To validate the theoretical prediction, several results in comparison with experimental data will follow.

4.1 Gradient of off-axis efforts at zero incidence angle

The theory for normal force and yaw moment gradients at small incidence angle has been well expressed in the original technical report [12]. The gradients are closed form solutions obtained by the analogy of a vertical fin having equal area as the projected area of propeller blades perpendicular to rotor disk and the analysis of deflected momentum. In the expressions, geometry of propeller blade was taken into consideration. Although the theory will only be briefly introduced and readers should refer to the original publication for detailed derivation, there are two incentives to present it here again : 1. To remind reader of the results for later usage ; 2. The original theory was developed for high-speed cruise condition, and a form more suitable for low-speed / hover conditions is presented.

The gradients are expressed in Eqs. 27, 28 with all velocity terms normalised by $\frac{\Omega D}{2\pi}$, and dynamic pressure terms by $\frac{1}{2}\rho \left(\frac{\Omega}{2\pi}\right)^2 D^2$, which is more appropriate for low-speed/hover conditions.

$$\frac{\partial C_N}{\partial \alpha_p}\bigg|_{\alpha_p=0} = \frac{\pi}{8} \frac{k_s f(a_i)\sigma I_1}{\frac{I_1}{I_1-\Delta}+k_a\sigma I_1} \tag{27}$$

$$\frac{\partial C_n}{\partial \alpha_p}\bigg|_{\alpha_p=0} = \frac{\pi}{8} \frac{k_s f(a_i)m}{1+k_a\sigma(I_1-\Delta)} \tag{28}$$

where a_i is the induced inflow ratio $2\pi\frac{V_i}{\Omega D}$. k_s and k_a are spinner factor and sidewash factor taken as constants $k_s = 1.14$ and $k_a = 0.4$ in current study, as suggested by Ribner. Their analytical definitions can be found in [13].

The function $f(a_i)$ is the effect of induced velocity V_{iA} on the dynamic pressure at propeller disk compared to $\frac{1}{2}\rho\left(\frac{\Omega}{2\pi}\right)^2 D^2$, defined in Eq. 29.

$$f(a_i) = \frac{J^{\frac{1}{2}}(J+a_i)\left[J(J+a_i)+(J+2a_i)^2\right]}{J^2+(J+2a_i)^2} \tag{29}$$

For other quantities in Eqs. 27, 28, we first introduce three integrations based on propeller blade geometry.

$$I_1 = \frac{3}{4}C_{L\alpha}\int_{\bar{r}_0}^1 \frac{c}{c_{0.75R}}\sin\beta' d\bar{r} \tag{30}$$

$$I_2 = \frac{3}{4}C_{L\alpha}\int_{\bar{r}_0}^1 \frac{c}{c_{0.75R}}\cos\beta' \bar{r} d\bar{r} \tag{31}$$

$$I_3 = \frac{3}{4}C_{L\alpha}\int_{\bar{r}_0}^1 \frac{c}{c_{0.75R}}\frac{\cos^2\phi}{\sin\phi}\bar{r}^2 d\bar{r} \tag{32}$$

where the mean lift line slope $C_{L\alpha}$ was approximated as $0.95 \times 2\pi$ in [12].

Δ and m are defined with these geometry integrals.

$$\Delta = \frac{\left(\sigma I_2 - 2\frac{a_i}{\pi}\right)\left(\sigma I_2 + 4\frac{a_i}{\pi}\right)}{\sigma(1+\sigma I_2)} \tag{33}$$

$$m = \frac{\sigma I_2 + 4\frac{a_i}{\pi}}{2(1+\sigma I_3)} \tag{34}$$

4.2 Off-axis efforts at high incidence

The off-axis effort gradients calculated from Ribner's theory agree with various experimental data for incidence angle up to $20°$. The linearity however doesn't hold for high incidence angle, and the change in local dynamic pressure and flow angle must be taken into consideration. In this section, a formulation of off-axis efforts at high incidence will be derived in detail for normal force. Expression for yaw moment can be derived in a similar procedure.

The normal force in downstream direction is mainly induced by the non-uniform tangential force distribution as the blade travels in one revolution. Tangential force is related with propeller torque. From Eq. 5, the local torque can be expressed in terms of local advance ratios.

$$\tilde{Q}(\psi) = \frac{\rho\Omega^2 D^5}{8\pi^3}K\sigma\sin\beta' A(\psi)B(\psi) \tag{35}$$

where factor $A(\psi)$ estimates the influence of local dynamic pressure change and factor $B(\psi)$ includes effect of local inflow angle variation implicitly. The two factors are calculated from Eqs. 36, 37.

$$A(\psi) = \left(1+\lambda'\sin\alpha_p\sin\psi\right)^2 \tag{36}$$

$$B(\psi) = \left(J_{0P} - \frac{J\cos\alpha_p}{1+\lambda'\sin\alpha_p\sin\psi}\right) \tag{37}$$

where $\lambda' = \frac{J}{\pi\bar{r}'}$ is the speed ratio at representative section.

The tangential force $\tilde{F}_T$ can be estimated by dividing the local torque by the representative radius r', and thus is proportional to torque $\tilde{Q}(\psi)$. For clarity in the following derivations, proportional constants will be neglected.

$$\tilde{F}_T(\psi) = \frac{\tilde{Q}(\psi)}{r'} \propto A(\psi)B(\psi) \tag{38}$$

For application of convertible aircraft, typically the speed ratio λ' can be regarded as of a smaller order than unity. Eq. 38 can be expanded and simplified by keeping only first order terms, and Eq. 39 is obtained after arithmetic manipulation.

$$\begin{aligned}\tilde{F}_T(\psi) \propto &(J_{0P}-J\cos\alpha_p)\\ &+\lambda'\sin\alpha_p\sin\psi(2J_{0P}-J\cos\alpha_p)\\ &+O\left(\lambda'^2\right)\end{aligned} \tag{39}$$

Assume the averaged normal force N is proportional to the mean of integrated tangential force along V_Z direction in one revolution.

$$N(\alpha_p, J) \propto \frac{1}{2\pi} \int_0^{2\pi} \tilde{F}_T(\psi) \sin\psi \, d\psi \qquad (40)$$

$$\propto J \sin\alpha_p (2J_{0P} - J\cos\alpha_p) \qquad (41)$$

Differentiate Eq. 41 with respect to incidence angle α_p and evaluate the normal force gradient at zero incidence.

$$\left.\frac{dN(\alpha_p, J)}{d\alpha_p}\right|_{\alpha_p=0} \propto J(2J_{0P} - J) \qquad (42)$$

Thus the evolution of normal force at high incidence can be evaluated as a ratio to normal force gradient at zero incidence with the same advance ratio. The resultant relation is a product of $\sin\alpha_p$ and advance ratio term.

$$\frac{N(\alpha_p, J)}{\partial N/\partial\alpha_p(0, J)} = \sin\alpha_p \frac{2J_{0P} - J\cos\alpha_p}{2J_{0P} - J} \qquad (43)$$

In a similar manner, the same relation can be obtained for yaw moment by using the azimuthal variation of local thrust. The off-axis efforts are expressed as coefficients in Eqs. 44, 45.

$$C_N = \frac{\partial C_N(\alpha_p = 0, J)}{\partial\alpha_p} \frac{2J_{0P} - J\cos\alpha_p}{2J_{0P} - J} \sin\alpha_p \qquad (44)$$

$$C_n = \frac{\partial C_n(\alpha_p = 0, J)}{\partial\alpha_p} \frac{2J_{0T} - J\cos\alpha_p}{2J_{0T} - J} \sin\alpha_p \qquad (45)$$

4.3 Validation of analytical expressions for off-axis efforts

The analytical expression for off-axis efforts are also compared to the two experimental database.

The theoretical results for normal force coefficient were plotted with experimental data from Yaggy et al. in Fig. 10 for the same operating condition as in section 3. The normal force coefficients initially increase with incidence in a quasi-linear fashion for all advance ratios, and then the force gradient starts to reduce. The force gradient is generally larger at higher advance ratio.

In Fig. 10, the theoretical result follows the increase well up to a high incidence angle close to the convergence region. Above it, the trend at high advance ratio tends to overestimate. Another notable feature is the existence of a local maximum point in normal force coefficient before 90°, which isn't captured in the theory.

The comparison for yaw moment coefficient was plotted in Fig. 11. The functional relation between yaw moment coefficient and incidence angle is very similar to that of normal force coefficient, except for the delay of local maximum, which for yaw moment coefficient lies
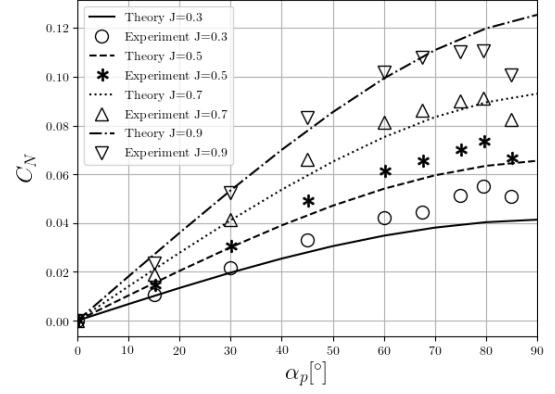

Figure 10: Normal force coefficient of No.1 propeller in [15] against incidence angle for various advance ratios
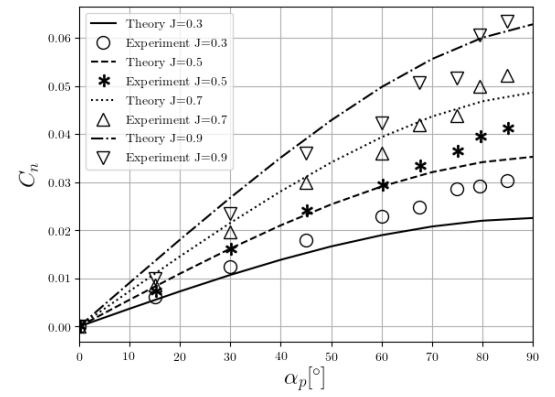

Figure 11: Yaw moment coefficient of No.1 propeller in [15] against incidence angle for various advance ratios

close to 90°. The close agreement between the theory and experimental data can also be observed in the figure.

The normal force coefficient for small-scale propeller is presented in Fig. 12. The model is in good agreement with experimental results. For small advance ratios, the model mostly resembles the behaviour of a sine function, with largest value obtained at 90°. For higher J, the advance ratio term becomes significant, and the normal force coefficient is larger than the $\sin\alpha_p$ correction.

Similar to the comparison with experimental database from Yaggy et al, there exists a local maximum in normal force coefficient for each advance ratio. The analytical model isn't capable to predict this peak, and the theoretical curve overshoot the experimental value after this local maximum.

In Fig. 13, the yaw moment coefficients from theoretical model and experimental measurement are plotted. The result demonstrated good trend and agreement for small advance ratios.

For $J \geq 0.7$, the theoretical value is overestimated. The difference is caused by the linear lift line assumption made at blade sections. The outer section of advancing
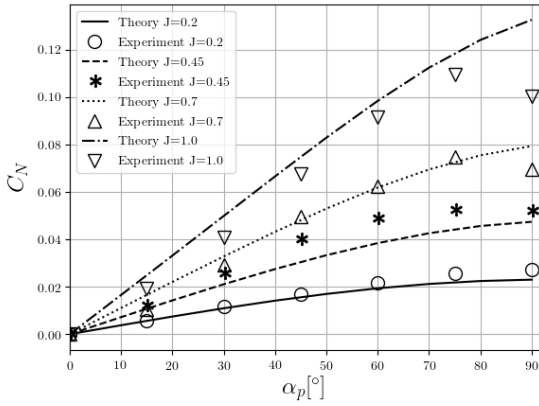
Figure 12: Normal force coefficient of a small-scale propeller against incidence angle for various advance ratios
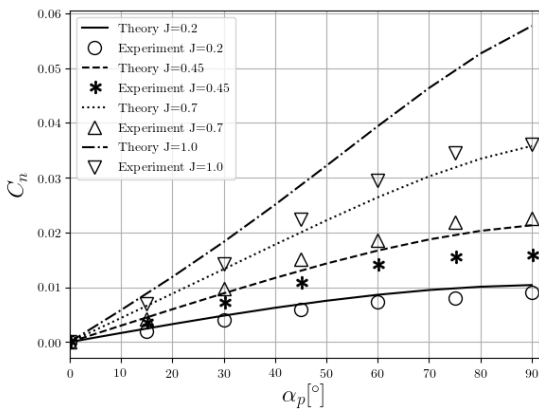

Figure 13: Yaw moment coefficient of a small-scale propeller against incidence angle for various advance ratios

blade is likely to stall at these advance ratios, and cannot sustain such a large yaw moment. The phenomenon is more pronounced for the drone propeller than the No.1 propeller in [15], because the latter was at cruise high-pitch setting. As a result, its zero-thrust advance ratio J_{0T} is significantly larger than the drone propeller, which reduces the influence of advance ratio term in Eq. 45, indicating less severe blade stall.

Despite the discrepancies between theoretical and experimental results at high advance ratio and/or high incidence angle, the model generally provides a reasonable estimation of propeller behaviours at off-design conditions for a fractional cost of higher-order methods.

5. CONCLUSION

The paper discussed an analytical model to predict propeller forces and moments at high incidence angle for a wide range of operating speed. The model is capable of estimating thrust, power, normal force and yaw moment coefficients, and is validated for incidence angle up to

90° and advance ratio up to $J = 1.0$. The model is inspired by the research from Ribner and De Young, and contains major modifications to accommodate both low-speed and high incidence conditions. The work is further completed by a comparison with experimental data of propellers at different scales over a wide range of testing parameters. Though discrepancies are noticeable at high advance ratio and/or very high incidence conditions, the model's consistency for different blade geometries and its highly-reduced calculation cost in predicting propeller performance at these challenging conditions make it very suitable for reduced-order applications such as preliminary design or system-level integration.

REFERENCES

[1] Murat Bronz, Ewoud J Smeur, Hector Garcia de Marina, and Gautier Hattenberger. Development of a fixed-wing mini uav with transitioning flight capability. Toulouse, France, June 2017. 35th AIAA Applied Aerodynamics Conference, AIAA AVIATION Forum.

[2] John De Young. Propeller at high incidence. *Journal of Aircraft*, 2(3):241–250, 1965.

[3] Alfred Gessow and Garry C Myers. *Aerodynamics of the Helicopter*. Macmillan New York, 1952.

[4] H Glauert. The stability derivatives of an airscrew. *British Aeronautical Research Council, Technical Report*, (642), 1919.

[5] R. G Harris. Forces on propeller due to sideslip. *British Aeronautical Research Council, Technical Report*, (427), 1918.

[6] Gordon J Leishman. *Principles of helicopter aerodynamics with CD extra*. Cambridge university press, 2006.

[7] Yuchen Leng, Thierry Jardin, Murat Bronz, and Jean-Marc Moschetta. Experimental analysis of propeller forces and moments at high angle of incidence. San Diego, United States, January 2019. AIAA Applied Aerodynamics Conference, AIAA SciTech Forum.

[8] Yuchen Leng, Heesik Yoo, Thierry Jardin, Murat Bronz, and Jean-Marc Moschetta. Aerodynamic modelling of propeller forces and moments at high angle of incidence. San Diego, United States, January 2019. AIAA Applied Aerodynamics Conference, AIAA SciTech Forum.

[9] Leandro Ribero Lustosa, François Defaÿ, and Jean-Marc Moschetta. Development of the flight model of a tilt-body mav. Toulouse, France, August 2014.

International Micro Air Vehicle Conference and Competition.

[10] David A Peters and Ninh HaQuang. Dynamic inflow for practical applications. *Journal of American Helicopter Society*, 33:64 – 68, October 1988.

[11] Warren F Phillips. *Mechanics of flight*. John Wiley & Sons, 2004.

[12] Herbert S Ribner. Formulas for propellers in yaw and charts of the side-force derivative. Technical Report NACA-TR-819, National Advisory Committee for Aeronautic. Langley Aeronautical Lab., Langley Field, VA, United States, January 1945.

[13] Herbert S Ribner. Propellers in yaw. Technical Report NACA-TR-820, National Advisory Committee for Aeronautic. Langley Aeronautical Lab., Langley Field, VA, United States, January 1945.

[14] R. Von Mises. *Theory of Flight*. Dover Books on Aeronautical Engineering Series. Dover Publications, 1959.

[15] Paul F Yaggy and Vernon L Rogallo. A wind-tunnel investigation of three propellers through an angle-of-attack range from 0 deg to 85 deg. Technical Report NACA-TN-D-318, NASA Ames Research Center, Moffett Field, CA, United States, May 1960.